



Functional tensor network solving many-body Schrödinger equationRui Hong, Ya-Xuan Xiao, Jie Hu, An-Chun Ji, and Shi-Ju Ran ^{*}
Department of Physics, Capital Normal University, Beijing 100048, China (Received 31 January 2022; revised 31 March 2022; accepted 31 March 2022; published 12 April 2022)

Solving the many-body Schrödinger equation in continuous spaces with the presence of strong correlations is an extremely important and challenging issue in quantum physics. In this work, we propose the functional tensor network (FTN) approach to solve the many-body Schrödinger equation. Provided the orthonormal functional bases, we represent the coefficients of the many-body wave function as a tensor network. The observables, such as energy, can be calculated simply by tensor contractions. Simulating the ground state becomes solving a minimization problem defined by the tensor network. An efficient gradient-descent algorithm based on automatically differentiable tensors is proposed. We here take the matrix product state (MPS), whose complexity scales only linearly with the system size, as an example. We apply our approach to solve the ground state of coupled harmonic oscillators and achieve high accuracy by comparing our results with the exact solutions. Reliable results are also given in the presence of three-body interactions, where the system cannot be decoupled from isolated oscillators. Our approach is simple and, with well-controlled error, essentially different from highly nonlinear neural-network solvers. Our work extends the applications of the tensor network from quantum lattice models to systems in continuous space. The FTN can be used as a general solver of the differential equations with many variables. The MPS exemplified here can be generalized to, e.g., fermionic tensor networks to solve the electronic Schrödinger equation.

DOI: [10.1103/PhysRevB.105.165116](https://doi.org/10.1103/PhysRevB.105.165116)**I. INTRODUCTION**

Solving differential equations belongs to the most fundamental but challenging tasks in mathematics, physics, etc. In general, the situations where we have exact solutions are extremely rare; thus, various analytical and numerical methods have been developed using simplifications or approximations to different extents.

Let us concentrate on quantum physics, where the Schrödinger equation plays a fundamental role. Different approximative treatments of this equation have evolved into different subfields. For instance, density functional theories and so-called *ab initio* calculations (see, e.g., [1,2]) successfully predict the properties of countless quantum matters ranging from molecules to solids under the assumption of weak correlations. Recently, the hybridization with machine learning has triggered a new upsurge in studying the Schrödinger equation, including simulations of ground states by better considering correlations [3–7] and inversely predicting the potentials knowing the wave functions or relevant physical information [8–11].

Towards strongly correlated cases, an important direction is simplifying to quantum lattice models, such as Heisenberg or Hubbard models on discretized lattices. Among the successful algorithms, remarkable progress has been made based on tensor networks (TNs) [12–16]. As two important examples, we have the density matrix renormalization group (DMRG) for simulating the ground states of one- and quasi-

one-dimensional systems [17–21] and projected-entangled pair states for the higher-dimensional ones [22,23].

The success of TNs lies in their high efficiency of representing quantum many-body states as well as powerful algorithms to deal with the TN calculations. On the cost of obeying the area law of entanglement entropy [22,24,25], TNs reduce the exponential complexity of representing a many-body state to a polynomial. Accurate results are obtained by TNs, thanks to the fact that for most models we are interested in, such as those with local interactions in one dimension [26], the area law holds. A TN was also proposed to solve the Schrödinger equation with discretized grid approximations [27–31]. However, beyond quantum lattices or grids, TNs for those with continuous variables are mainly concentrated on quantum fields [32–37]. The systematic use of TNs for solving differential equations with many continuous variables has barely been explored.

In this work, a TN is proposed to solve the many-body Schrödinger equation in continuous space. Given the orthonormal functional bases, the coefficients of the quantum wave function are represented in the form of a TN. Defining the loss function L as the energy, the automatic differentiation technique [38] is utilized to achieve the TN representing the ground state. We dub this approach the *functional TN*. Taking the matrix product state (MPS), which is a special one-dimensional TN [12], as an example, our approach is illustrated in Fig. 1. The loss function is calculated as the inner product of two MPSs. One MPS is the summation of many MPSs representing the wave function acted on by the corresponding operators, and the other is the MPS representing the wave function itself. The tensors forming the

*Corresponding author: sjran@cnu.edu.cn

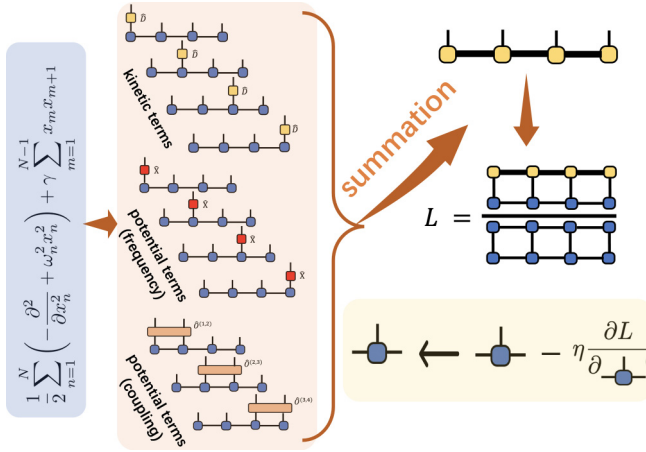


FIG. 1. An illustration of the functional MPS approach. By representing the trial wave function in MPS, the loss function L becomes the inner product of two MPSs. One MPS is the summation of several MPSs, each of which results from the trial wave function acted upon by an operator. The inset illustrates the gradient descent [Eq. (29)] to update the tensors in the trial MPS.

MPS are automatically differentiable and are updated by the gradient-descent algorithm. The gradients are obtained in the back-propagation process [38], similar to optimizations of neural networks.

We test our approach on coupled harmonic oscillators with two- and three-body interactions [see Eq. (27)]. The model cannot be decoupled to isolated oscillators in the presence of three-body terms. With only the two-body interactions, high accuracy is demonstrated by comparing the achieved ground-state energy to the exact one. The error is well controlled by the entanglement of the MPS. The ground-state energy and entanglement entropy with the three-body terms are also demonstrated. Compared with solvers of differential equations based on neural networks [39–43] that are, in general, highly nonlinear, our functional TN solver does not require sampling or training data and thus does not belong to the “data-driven” solvers. The optimizations of TN are implemented simply by tensor contractions. Our work sheds light on using a TN as an efficient solver of general many-variable differential equations in and beyond quantum physics.

II. PRELIMINARIES AND NOTATIONS

A. Basis and expansion

With a set of orthonormal functional bases $\{\phi_s(x)\}$ satisfying $\int_{-\infty}^{\infty} \phi_s^*(x)\phi_s(x)dx = \delta_{s's}$, a given function $\psi(x)$ can be expanded as

$$\psi(x) = \sum_{s=0}^{\mathcal{D}-1} C_s \phi_s(x), \quad (1)$$

where C_s denotes the expansion coefficients and \mathcal{D} is the expansion order. Here, we assume $\psi(x)$ is smooth.

Considering $\psi(x)$ as the wave function of a quantum system, it should satisfy the normalization condition as $\int_{-\infty}^{\infty} \psi^*(x)\psi(x)dx = 1$. Thanks to the orthonormal condition of the basis, the normalization condition can be represented

by the $L2$ norm of the coefficients as

$$|\mathbf{C}| = \sqrt{\sum_s |C_s|^2} = 1. \quad (2)$$

Note we use a bold letter, such as \mathbf{C} , to denote a vector, matrix, or tensor and use the same letter with subscripts to denote its elements, such as the s th element C_s .

B. Operations

Consider an operator, denoted \hat{O} , that satisfies the linear condition in the functional space as

$$\hat{O}\psi(x) = \hat{O} \sum_s C_s \phi_s(x) = \sum_s C_s \hat{O}[\phi_s(x)]. \quad (3)$$

Assume for each basis function $\phi_s(x)$ that \hat{O} satisfies

$$\hat{O}[\phi_s(x)] = \sum_{s'=0}^{\mathcal{D}-1} O_{s's} \phi_{s'}(x). \quad (4)$$

Apparently, the expansion coefficients of the function $\tilde{\psi}(x) = \hat{O}[\psi(x)] = \sum_s \tilde{C}_s \phi_s(x)$ satisfy

$$\tilde{C}_{s'} = \sum_s O_{s's} C_s. \quad (5)$$

In general, $O_{s's}$ can be numerically evaluated as

$$O_{s's} = \int_{-\infty}^{\infty} \phi_{s'}^*(x) \hat{O}[\phi_s(x)] dx. \quad (6)$$

In some special cases, the matrix $O_{s's}$ given the basis $\{\phi_s(x)\}$ can be solved analytically. As an example, let us take $\phi_s(x)$ as the s th eigenstate of the quantum harmonic oscillator with the Hamiltonian

$$\hat{H}^{\text{HO}} = -\frac{1}{2} \frac{d^2}{dx^2} + \frac{x^2}{2}. \quad (7)$$

We take the Plank constant $\hbar = 1$ for simplicity. We have

$$\phi_s(x) = \left(\frac{1}{2^s s! \sqrt{\pi}} \right)^{\frac{1}{2}} e^{-\frac{x^2}{2}} h_s(x), \quad (8)$$

with $h_s(x)$ being the Hermitian polynomial. We dub Eq. (8) the single-oscillator basis (SOB). Obviously, $\{\phi_s(x)\}$ satisfy the orthonormal conditions.

We now consider the operation $\hat{D} = \frac{d}{dx}$. With $D_{s's} = \int_{-\infty}^{\infty} \phi_{s'}^*(x) \hat{D}[\phi_s(x)] dx$ [Eq. (6)], we have

$$D_{s's} = \begin{cases} \sqrt{\frac{s}{2}}, & s' = s - 1, \\ -\sqrt{\frac{s+1}{2}}, & s' = s + 1. \end{cases} \quad (9)$$

The dimensions of the matrix \mathbf{D} should be infinite (i.e., $\mathcal{D} \rightarrow \infty$) to exactly represent the differential operator. In practice, one may use a proper approximation by taking a finite \mathcal{D} . For the k -order differentiation, we have

$$\int_{-\infty}^{\infty} \phi_{s'}^*(x) \hat{D}^k[\phi_s(x)] dx = [\mathbf{D}^k]_{s's}, \quad (10)$$

with \mathbf{D}^k being the k th power of the matrix \mathbf{D} . Another example is the operation $\hat{X} = x$. Similarly, we have

$$X_{s's} = \begin{cases} \sqrt{\frac{s}{2}}, & s' = s - 1, \\ \sqrt{\frac{s+1}{2}}, & s' = s + 1. \end{cases} \quad (11)$$

C. Solving a differential equation by optimization

Consider a differential equation formed by P terms. We can formally write it as

$$\sum_{p=1}^P \hat{O}^{[p]}[\psi(x)] = 0. \quad (12)$$

Let us take the static Schrödinger equation as an example; we have

$$\begin{aligned} \hat{O}^{[1]} &= -\frac{1}{2} \frac{d^2}{dx^2}, \\ \hat{O}^{[2]} &= V(x), \\ \hat{O}^{[3]} &= -E. \end{aligned} \quad (13)$$

The first two terms (kinetic and potential terms, respectively) correspond to the Hamiltonian $\hat{H} = \hat{O}^{[1]} + \hat{O}^{[2]}$, and the third corresponds to the (negative) energy.

To solve the static Schrödinger equation, we regard the coefficients C_s in $\psi(x) = \sum_s C_s \phi_s(x)$ as the variational parameters. Now we consider the calculation of the ground state, i.e., the eigenfunction with the lowest eigenvalue (energy) of the given Hamiltonian. With the normalization constraint of the wave function given in Eq. (2), the energy (quantum average of \hat{H}) satisfies

$$E = \langle \hat{H} \rangle = \int_{-\infty}^{\infty} \psi^*(x) \hat{H} \psi(x) dx = \sum_{s's} C_s^* H_{ss'} C_{s'}, \quad (14)$$

where $H_{ss'}$ can be calculated using Eq. (6). We define the loss function

$$L = \frac{E}{|\mathbf{C}|^2}. \quad (15)$$

We introduce the division over $|\mathbf{C}|^2$ so that we do not need to consider the normalization of $\psi(x)$ in the optimization process. Then \mathbf{C} is iteratively updated using gradient descent as

$$\mathbf{C} \leftarrow \mathbf{C} - \eta \frac{\partial L}{\partial \mathbf{C}}, \quad (16)$$

with η being the learning rate or gradient step.

Beyond the static Schrödinger equation, we can use gradient descent to solve the differential equation given in Eq. (12). In a given set of functional bases, the differential equation can be written as

$$\sum_{ps's} O_{s's}^{[p]} C_s \phi_{s'}(x) = 0. \quad (17)$$

Since $\{\phi_s(x)\}$ is a set of orthonormal bases, we have

$$\sum_{ps} O_{s's}^{[p]} C_s = 0 \quad \forall s'. \quad (18)$$

We introduce the vector \mathbf{Z} with its s' th element $Z_{s'} = \sum_{ps} O_{s's}^{[p]} C_s$. With $|\mathbf{Z}|^2 = 0$, $\psi^*(x)$ is the solution

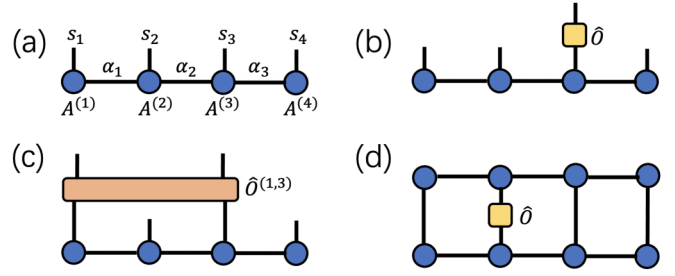


FIG. 2. (a) A graph of an MPS [Eq. (21)] with its physical and virtual bonds. The virtual bonds at the two ends are one-dimensional and thus are ignored in the graph. In (b) and (c), we illustrate the actions of one- and two-body operators on the MPS. In (d) we illustrate the average of a one-body operator $\langle \hat{O} \rangle$.

of the differential equation. Therefore, we define the loss function as

$$\mathcal{L} = |\mathbf{Z}|^2. \quad (19)$$

The coefficients can be updated using Eq. (16).

III. FUNCTIONAL MATRIX PRODUCT STATE

A. Matrix product state representation for the coefficients of a multivariable function

Given N sets of orthonormal bases $\{\phi_{s_n}(x_n)\}$, a function with N independent variables $\mathbf{x} = (x_1, \dots, x_N)$ can be expanded as

$$\psi(\mathbf{x}) = \sum_{s_1 \dots s_N=0}^{\mathcal{D}-1} C_{s_1 \dots s_N} \phi_{s_1}(x_1) \cdots \phi_{s_N}(x_N). \quad (20)$$

Obviously, the complexity of the coefficient tensor \mathbf{C} scales exponentially with the number of variables N as $O(\mathcal{D}^N)$.

One key of our proposal is using the TN to represent the coefficients. As illustrated in Fig. 2(a), we take MPSs as an example and have

$$C_{s_1 \dots s_N} = \sum_{\alpha_0 \dots \alpha_{N-1}}^{\chi-1} A_{\alpha_0 s_1 \alpha_1}^{(1)} A_{\alpha_1 s_2 \alpha_2}^{(2)} \cdots A_{\alpha_{N-1} s_N \alpha_N}^{(N)}, \quad (21)$$

with $\{\alpha_n\}$ being the virtual bonds. We take the MPS to have open boundary conditions in the whole paper, with $\dim(\alpha_0) = \dim(\alpha_N) = 1$. The upper bound of $\dim(\alpha_n)$ ($n = 1, \dots, N-1$) is called the virtual bond dimension of the MPS, denoted by χ . The indexes $\{s_n\}$ are called the physical bonds, and the dimension is called the physical bond dimension. In our cases, we have $\dim(s_n) = \mathcal{D}$, i.e., the expansion order. The number of parameters in the MPS (i.e., the total number of elements in the tensors $\{\mathbf{A}^{(n)}\}$ for $n = 1, \dots, N$) scales only linearly with N as $O(N\mathcal{D}\chi^2)$, while that of \mathbf{C} scales exponentially as $O(\mathcal{D}^N)$.

Akin to the one-variable cases, the norm of $\psi(\mathbf{x})$ equals the norm of the coefficient tensor (or MPS), i.e.,

$$\int_{-\infty}^{\infty} \psi^*(\mathbf{x}) \psi(\mathbf{x}) d\mathbf{x} = \sum_{s_1, \dots, s_N} C_{s_1, \dots, s_N}^* C_{s_1, \dots, s_N} = |\mathbf{C}|^2, \quad (22)$$

with $d\mathbf{x} = \prod_{n=1}^N dx_n$. Note that when the tensors in the MPS $\{\mathbf{A}^{(n)}\}$ are given, $|\mathbf{C}|^2$ can be obtained without calculating \mathbf{C} . Therefore, the exponential complexity is avoided. Notably, the proposed method and discussion in this work can be readily extended generally to other TNs.

B. Operations and quantum average

Consider an operation $\hat{O}^{(m)}$ on x_m . According to the linearity and the independence of the variables, we have

$$\begin{aligned} \tilde{\psi}(\mathbf{x}) &= \hat{O}^{(m)}[\psi(\mathbf{x})] \\ &= \sum_{s_1 \cdots s_N=0}^{\mathcal{D}-1} C_{s_1, \dots, s_N} \left[\prod_{n \neq m} \phi_{s_n}(x_n) \right] \hat{O}^{(m)}[\phi_{s_m}(x_m)]. \end{aligned} \quad (23)$$

We denote the tensors in the MPS representing $\tilde{\psi}(\mathbf{x})$ as $\{\tilde{\mathbf{A}}^{(n)}\}$. Given the tensors $\{\mathbf{A}^{(n)}\}$ in the MPS representation of $\psi(\mathbf{x})$, we have $\mathbf{A}^{(n)} = \tilde{\mathbf{A}}^{(n)}$ for $n \neq m$. For $n = m$, we have

$$\tilde{A}_{\alpha s \alpha'}^{(m)} = \sum_{s'} O_{ss'}^{(m)} A_{\alpha s' \alpha'}^{(m)}, \quad (24)$$

where $O_{ss'}^{(m)}$ satisfies Eq. (6). See Fig. 2(b) for an illustration.

Similarly, the MPS obtained by acting on multiple operators can be derived. Take two operators, $\hat{O}^{(m_1)}$ and $\hat{O}^{(m_2)}$, as an example. The tensors $\{\tilde{\mathbf{A}}^{(n)}\}$ in the MPS representing $\tilde{\psi}(\mathbf{x}) = \hat{O}^{(m_2)} \hat{O}^{(m_1)} \psi(\mathbf{x})$ satisfy $\tilde{\mathbf{A}}^{(n)} = \mathbf{A}^{(n)}$ for $n \neq m_1$ and $n \neq m_2$, and $\tilde{A}_{\alpha s \alpha'}^{(n)} = \sum_{s'} O_{ss'}^{(n)} A_{\alpha s' \alpha'}^{(n)}$ for $n = m_1$ or $n = m_2$.

Consider an operator acting on multiple variables, such as $\hat{O}^{(m_1, m_2)}$ acting on x_{m_1} and x_{m_2} . We assume that $\hat{O}^{(m_1, m_2)}$ cannot be decomposed to the product of two single-variable operators, i.e., $\hat{O}^{(m_1)} \hat{O}^{(m_2)}$. Then as an extension of Eq. (6), we introduce a fourth-order tensor $\mathbf{O}^{(m_1, m_2)}$, whose elements satisfy

$$\begin{aligned} O_{n'_1 n'_2 n_1 n_2}^{(m_1, m_2)} &= \int_{-\infty}^{\infty} \phi_{n'_1}^*(x_{m_1}) \phi_{n'_2}^*(x_{m_2}) \\ &\quad \times \hat{O}^{(m_1, m_2)}[\phi_{n_1}(x_{m_1}) \phi_{n_2}(x_{m_2})] dx_{m_1} dx_{m_2}. \end{aligned} \quad (25)$$

The calculation of the MPS representing $\tilde{\psi}(\mathbf{x}) = \hat{O}^{(m_1, m_2)}[\psi(\mathbf{x})]$ is illustrated in Fig. 2(c). The actions of multivariable operators can be similarly defined.

Consider the quantum average of the operator $\hat{O}^{(m)}$ as

$$\langle \hat{O} \rangle = \int_{-\infty}^{\infty} \psi^*(\mathbf{x}) \hat{O}^{(m)}[\psi(\mathbf{x})] d\mathbf{x}. \quad (26)$$

As illustrated in Fig. 2(d), $\langle \hat{O} \rangle$ is calculated in the same way as calculating the average of a single-site operator with a standard MPS, similar to Eq. (14). The same arguments can be made for the quantum average of multivariable operators.

C. Solving coupled harmonic oscillators

We consider the following N coupled harmonic oscillators in one dimension as an example, where the Hamiltonian reads

$$\begin{aligned} \hat{H}^{\text{HO}} &= \frac{1}{2} \sum_{n=1}^N \left(-\frac{\partial^2}{\partial x_n^2} + \omega_n^2 x_n^2 \right) + \gamma \sum_{m=1}^{N-1} x_m x_{m+1} \\ &\quad + \tilde{\gamma} \sum_{m=1}^{N-2} x_m x_{m+1} x_{m+2}, \end{aligned} \quad (27)$$

where ω_n gives the natural frequency of the n th oscillator and γ and $\tilde{\gamma}$ are the two- and three-body coupling constants, respectively.

We choose the bases $\{\phi_{s_n}(x_n)\}$ as the SOB [Eq. (8)], considering that the matrices of the required operators, namely, \hat{D} and \hat{X} , can be analytically obtained [Eqs. (9) and (11)]. We suppose the ground state $\psi(\mathbf{x})$ we aim to obtain is written in the MPS formed by the tensors $\{\mathbf{A}^{(n)}\}$. For the kinetic terms, we define $\tilde{\psi}^{\text{K}(m)}(\mathbf{x}) = -\frac{1}{2} \frac{\partial^2}{\partial x_m^2} \psi(\mathbf{x})$. According to Sec. III B, the tensors of the MPS representing $\tilde{\psi}^{\text{K}(m)}$ can be obtained, where the m th tensor should be changed to

$$\tilde{A}_{\alpha s \alpha'}^{(m)} = -\frac{1}{2} \sum_{s''} D_{ss''} D_{s''\alpha'} A_{\alpha s'' \alpha'}^{(m)}, \quad (28)$$

with \mathbf{D} being the coefficient matrix of the differential operator \hat{D} in the SOB [Eq. (9)]. Note the coefficients of operators depend on only the choice of the basis [Eq. (6)], instead of the number of variables or the form representing the coefficients of the wave functions.

For the potential terms, we define $\tilde{\psi}^{\text{P}(m)}(\mathbf{x}) = \frac{1}{2} \omega_n^2 x_m^2 \psi(\mathbf{x})$. Similarly, the MPS representation of $\tilde{\psi}^{\text{P}(m)}$ can be obtained from $\{\mathbf{A}^{(n)}\}$ and \mathbf{X} by using Eq. (11). For the coupling terms, we define $\tilde{\psi}^{\text{C}(m, m+1)}(\mathbf{x}) = \gamma x_m x_{m+1} \psi(\mathbf{x})$. The m th and $(m+1)$ th tensors should be calculated following Eq. (24). The MPSs corresponding to the three-body interactions can be similarly defined.

In all, we have $(4N-3)$ MPSs, in which N MPSs are from the kinetic terms, N are from the frequency terms, and $(2N-3)$ are from the coupling terms. The summation of these MPSs results in the MPS that represents $\tilde{\psi}^{\text{H}}(\mathbf{x}) := \hat{H} \psi(\mathbf{x})$. Two MPSs with the same physical bond dimension can be added, which results in an MPS with the same physical bond dimension. Therefore, we can obtain $\tilde{\psi}^{\text{H}}(\mathbf{x})$ as an MPS. Denoting the virtual bond dimensions of two added MPSs as χ_1 and χ_2 , respectively, the virtual bond dimension of the resulting MPS satisfies $\chi \leq \chi_1 + \chi_2$. The virtual bond dimension (denoted as χ_{H}) of $\tilde{\psi}^{\text{H}}(\mathbf{x})$ satisfies $\chi_{\text{H}} \leq (4N-3)\chi$, with χ being the virtual bond dimension of $\psi(\mathbf{x})$. Since the MPSs in the additions have many shared tensors, we, in fact, have $\chi_{\text{H}} \ll (4N-3)\chi$. See Appendix B for more details.

To obtain the ground state, we choose the energy in Eq. (15) as the loss function L . With a trial MPS (where the tensors can be initialized randomly), L can be calculated with polynomial complexity, avoiding the exponentially large full coefficient tensor. For instance, the energy [Eq. (14)] is obtained by the inner product of the MPSs $\psi(\mathbf{x})$ and $\tilde{\psi}^{\text{H}}(\mathbf{x})$. The illustration of the inner product is similar to Fig. 2(d). The complexity of calculating the inner product of two MPSs generally scales as $O[N\mathcal{D}\chi\chi_{\text{H}}(\chi + \chi_{\text{H}})]$. See Appendix C for more details.

After calculating the loss L , the tensors in the MPS representing the wave function $\psi(\mathbf{x})$ can be updated by the gradient descent as

$$\mathbf{A}^{(n)} \leftarrow \mathbf{A}^{(n)} - \eta \frac{\partial L}{\partial \mathbf{A}^{(n)}}, \quad (29)$$

where the gradients $\frac{\partial L}{\partial \mathbf{A}^{(n)}}$ can be obtained by the automatic differentiation technique of the TN [38]. In practice, we obtain the gradients for all tensors and update them simultaneously in

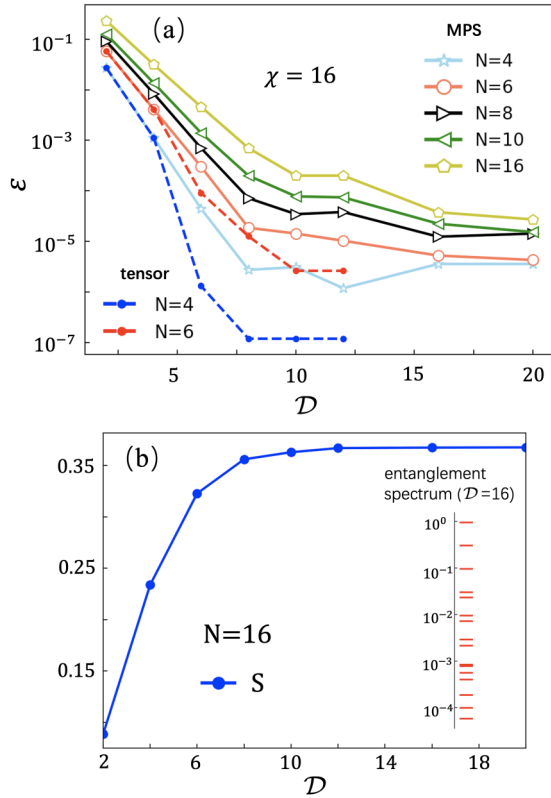


FIG. 3. (a) The error of the ground-state energy ε [Eq. (30)] versus the expansion order D for the coupled harmonic oscillators with $\gamma = -0.5$ and $\tilde{\gamma} = 0$ [Eq. (27)]. We vary the number of oscillators from $N = 4$ to 16 and fix the virtual bond dimension of the MPS to $\chi = 16$. The results obtained by optimizing the full coefficient tensors are shown by the solid symbols with dashed lines. In (b) we give the entanglement entropy S [Eq. (32)] versus D for $N = 16$. The inset shows the entanglement spectrum (Schmidt numbers) measured in the middle of the MPS for $D = 16$.

a back-propagation process. We choose the Adam optimizer [44] to control the learning rate η . After sufficiently many iterations of updates, L converges to the ground-state energy, and $\psi(\mathbf{x})$ converges to the ground state. Compared with the solvers of differential equations based on neural networks that are highly nonlinear [39–43], one advantage of our functional MPS (and general TN) solver is that sampling is not required. The optimization is implemented simply by tensor contractions.

IV. NUMERICAL RESULTS

Taking $\gamma = 0.5$ and $N = 4, 6, \dots, 20$ as examples, the Hamiltonian in Eq. (27) can be exactly solved by decoupling to isolated oscillators. Note that we fix $\omega_n = 1$ in our simulations. Figure 3 demonstrates the error of the ground-state energy

$$\varepsilon = |E - E_{\text{exact}}|, \quad (30)$$

where E_{exact} is the exact solution satisfying [45]

$$E_{\text{exact}} = \frac{1}{2} \sum_{n=1}^N \sqrt{1 + 2\gamma \cos\left(\frac{n\pi}{N+1}\right)}. \quad (31)$$

The open symbols with solid lines show the results of the function MPS method with bond dimensions $\chi = 16$. For comparison, the solid symbols with dashed lines show the results of directly treating the coefficients as a D^N -dimensional tensor (as explained in Sec. II C). For about $N < 8$, the differences between the results for the MPS and for the tensor are small. This indicates that the errors are mainly from the finiteness of the expansion order D (the physical bond dimension of the MPS). The error decreases with increasing D and approximately converges for about $D > 12$. For the relatively large D , the errors from using the MPS are lower than those for the tensor due to the finiteness of χ in the MPS (i.e., truncation error). The differences are still slight [$\sim(O^{-5})$ or less].

Another critical advantage of our approach over the neural-network solvers is the interpretability. Below, we consider the entanglement of MPS. Thanks to the orthonormal property of the functional bases, the entanglement of the MPS representing the coefficients of the wave function shares the same quantum probabilistic interpretation of the MPS representing the quantum states of lattice models. In specific, it characterizes the “quantum version” of correlations between two subsystems. By “subsystem” in our examples, we mean a subset of oscillators.

In addition to characterizing the quantum correlations among oscillators, entanglement also characterizes the truncation error of MPSs induced by the finiteness of χ . The entanglement entropy is defined as

$$S = -2 \sum_{k=0}^{\chi-1} \lambda_k^2 \ln \lambda_k, \quad (32)$$

with λ_k being the k th number in the entanglement spectrum or the k th Schmidt number. The upper bound of S for an MPS with virtual bond dimension χ satisfies $S \sim \ln \chi$. Considering an extreme case with $S = 0$, there will be only one nonzero Schmidt number. The state will be a product state $\psi(\mathbf{x}) = \prod_n [\sum_{s_n} C_{s_n}^{(n)} \phi_{s_n}(x_n)]$, and the coefficient tensor will be a rank-1 tensor satisfying $\mathbf{C} = \prod_{\otimes} \mathbf{C}^{(n)}$. For $S > 0$, the truncation error in general has the same or a smaller order of magnitude as the smallest Schmidt number. Obviously, we always have $S > 0$ for the electronic wave functions in order to respect the anticommutation relations. We leave electronic systems to a future study.

Figure 3(b) shows the entanglement entropy S against D , where we measure S in the middle of the MPS. In other words, S gives the entanglement entropy between the first $N/2$ oscillators and the rest (we take N to be even, without losing generality). As D increases, S converges to about 0.36, indicating that the ground state is not highly entangled. The inset shows the entanglement spectrum for $D = 16$. The smallest number in the spectrum is about $O(10^{-5})$, which is consistent with the error ε .

To further control the truncation error, Fig. 4 shows that the error of energy ε converges to $O(10^{-5})$ for $\chi \geq 16$ (with $D = 8$). When N increases, ε will generally increase slightly, with χ remaining the same. The inset shows the entanglement entropy S increases with χ , meaning more entanglement will be captured (more product states are contained in the overlap) with larger χ . S converges to about $S \simeq 0.36$ for $\chi \geq 16$.

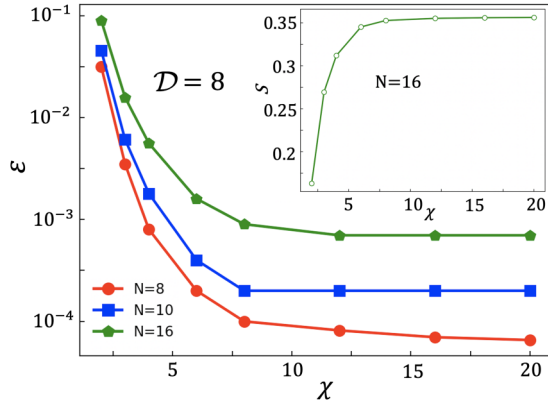


FIG. 4. The error of the ground-state energy ε [Eq. (30)] and entanglement entropy S [inset; see Eq. (32)] versus the virtual bond dimension χ . We take $\mathcal{D} = 8$, $\gamma = -0.5$, and $\tilde{\gamma} = 0$.

With different coupling strengths, there is not always a “physical” solution. Assuming γ is a real number, the Hamiltonian is Hermitian, and the energy (an eigenvalue) should be real. From the analytical solution given by Eq. (31), a real solution exists for $|\gamma| < \gamma_c$, with

$$\gamma_c = \frac{1}{2} \sec \frac{\pi}{N+1}. \quad (33)$$

However, the MPS still gives a converged energy even when a real ground-state energy does not exist. As shown in Fig. 5, the obtained energy matches accurately the exact value when the real energy exists. To numerically identify the region with no physical solution, we calculate the loss \mathcal{L} defined in Eq. (19), which characterizes the violation of the Schrödinger equation. In the inset of Fig. 5, we show that \mathcal{L} identifies the regions with or without a physical solution, where we have $\mathcal{L} \gg 0$ for $|\gamma| > \gamma_c$.

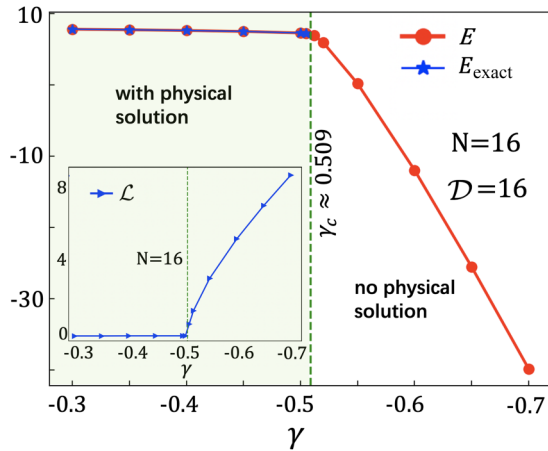


FIG. 5. The ground-state energy obtained with our method E and with the exact solution E_{exact} with $N = 16$. For $|\gamma| > \gamma_c = \frac{1}{2} \sec \frac{\pi}{17} \simeq 0.509$, there is no real solution for the ground-state energy. The inset shows that this region can be identified by the loss \mathcal{L} defined in Eq. (19), where we have $\mathcal{L} \gg 0$ for $|\gamma| > \gamma_c$. We take $N = 16$ and $\mathcal{D} = 16$.

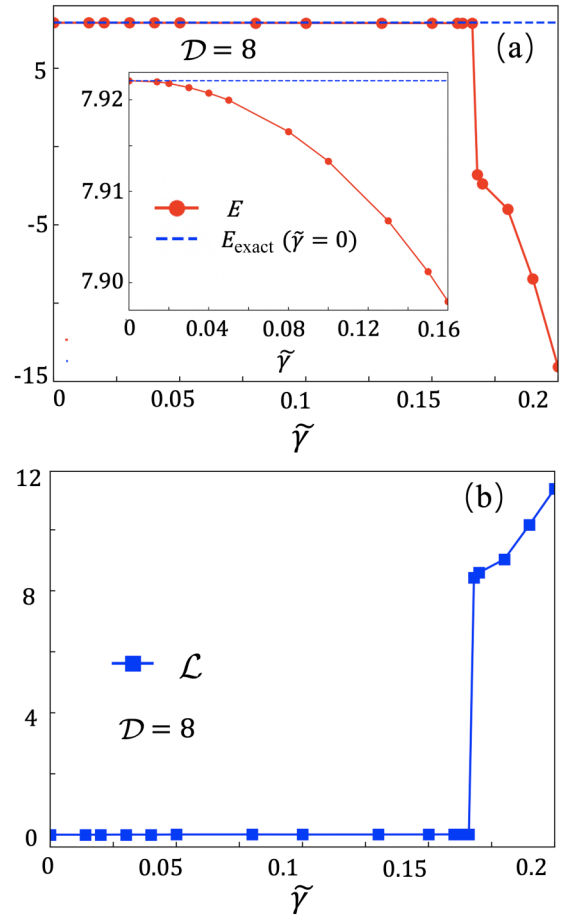


FIG. 6. (a) The ground-state energy E obtained with our function MPS method versus the strength of the three-body interactions $\tilde{\gamma}$. We take $N = 16$, $\mathcal{D} = 8$, $\chi = 16$, and $\gamma = -0.2$. The dashed line shows the exact energy E_{exact} for $\tilde{\gamma} = 0$. The inset shows E for $\tilde{\gamma} < \tilde{\gamma}_c \simeq 0.168$, where a real solution for the ground-state energy exists. In (b), we show that the loss \mathcal{L} [Eq. 19] suddenly becomes $\gg 1$ for $\tilde{\gamma} > \tilde{\gamma}_c$.

Figure 6(a) shows the ground-state energy E obtained with our function MPS method for different three-body interaction strengths $\tilde{\gamma}$ with $N = 16$, $\mathcal{D} = 8$, $\chi = 16$, and $\gamma = -0.2$. We identify that for about $\tilde{\gamma} < \tilde{\gamma}_c \simeq 0.168$, E changes smoothly with $\tilde{\gamma}$, as demonstrated in the inset. At $\tilde{\gamma} \simeq \tilde{\gamma}_c$, E drastically jumps to a negative number. From Fig. 6(b), we can see that \mathcal{L} suddenly becomes $\gg 1$ for $\tilde{\gamma} > \tilde{\gamma}_c$. This implies the real solution does not exist in this region.

V. SUMMARY AND PERSPECTIVE

In this work, we extended the utilization of TNs to solving the many-body Schrödinger equation in continuous space. Given the local functional bases, the coefficients of the wave function were given in the form of a TN, where the exponential complexity is reduced to a polynomial. The observables such as energy can be calculated simply by tensor contractions. Automatically differentiable tensors were used to form the TN. Their gradients can be obtained in a back-propagation process and can be used to minimize the energy using gradient descent. The error of the ground-state simulation was well controlled by the entanglement. We took the TN to be

a MPS as an example and applied it to the coupled harmonic oscillators with two- and three-body interactions. The existence of a physical solution can be identified by the loss that characterizes the violation of the Schrödinger equation.

Our proposal can be readily extended to general differential equations with many variables. The functional bases can be replaced by others, such as the Taylor series, depending on the convenience of solving the target equation. The MPS can also be generalized to other TNs such as projected entangled pair states. For electrons, the fermionic TNs [46–49] can be used to represent the coefficients in order to respect the anticommutation relations. Our approach and the quantum chemistry DMRG algorithms [27,28,30,50] both belong to applications of the MPS to models in continuous space, which can bring complementary implications to each other. The functional TN aims more directly at solving general differential equations and here was applied to the Schrödinger equation in its very original form. For the interacting electrons, the functional TN can learn from the quantum chemistry DMRG about, e.g., the definitions of the basis in the second quantization picture and the optimization strategy. Besides entanglement, our work could build a bridge between the Schrödinger equation and concepts with close relevance to TNs, such as symmetries [51–54] and quantum computation (see, e.g., [55–59]).

ACKNOWLEDGMENTS

This work was supported by NSFC (Grants No. 12004266, No. 11834014, and No. 62175169), the Beijing Natural Science Foundation (Grant No. Z180013), the Foundation of Beijing Education Committees (Grant No. KM202010028013), and the key research project of the Academy for Multidisciplinary Studies, Capital Normal University.

APPENDIX A: NECESSARY NOTATIONS

Given an N th-order tensor \mathbf{T} , we use $T_{s_1 s_N \dots s_N}$ to represent a specific element. Take the following matrix (second-order tensor) \mathbf{M} as an example:

$$\mathbf{M} = \begin{bmatrix} 0 & 1 \\ 1 & 0 \end{bmatrix}. \quad (\text{A1})$$

We have matrix elements $M_{00} = M_{11} = 0$ and $M_{01} = M_{10} = 1$. Note to number multiple indexes or tensors, we start the numbering from 1. For a given index, say, χ -dimensional, we take its value from 0 to $\chi - 1$. The indexes of tensors are always subscripts. The superscripts, such as (n) in $\mathbf{A}^{(n)}$, are not actually indexes and are only to distinguish the symbols for different tensors.

We use a colon in the subscripts to represent the slice of tensor, following the syntax convention of PYTHON. For instance, $\mathbf{M}_{0,:} = [0, 1]$ is a vector that gives the zeroth row of \mathbf{M} . For the N th-order tensor \mathbf{T} , we use $\mathbf{T}_{s_1, \dots, s_{N-2}, :}$ to represent the matrix by fixing the first $(N - 2)$ indexes to (s_1, \dots, s_{N-2}) . The size of this matrix is $\dim(s_{N-1}) \times \dim(s_N)$. The range of the slice can be specified. Taking a vector \mathbf{V} as an example, $\mathbf{V}' = \mathbf{V}_{:a:b}$ [with a and b being two non-negative integers and $a < b < \dim(\mathbf{V})$] gives a $(b - a)$ -dimensional vector, satisfying $V'_n = V_{n+a}$ with $n = 0, \dots, b - a - 1$. Note $\mathbf{V}_{0:b}$ can be simplified to $\mathbf{V}_{:b}$, and $\mathbf{V}_{a:\dim(\mathbf{V})}$ can be simplified to $\mathbf{V}_{:a}$.

APPENDIX B: ADDITION OF MATRIX PRODUCT STATES

Given two MPSs formed by the tensors $\{\mathbf{A}^{(n)}\}$ and $\{\mathbf{B}^{(n)}\}$ ($n = 1, \dots, N$), the addition of these two MPSs can be written in the MPS form. We denote the tensors of the resulting MPS as $\{\mathbf{Q}^{(n)}\}$. In general, the elements of $\mathbf{Q}^{(n)}$ are zero except for the following parts:

$$\begin{aligned} \mathbf{Q}_{:\chi_1, \dots, \chi'_1}^{(n)} &= \mathbf{A}^{(n)}, \\ \mathbf{Q}_{\chi_1, \dots, \chi'_1}^{(n)} &= \mathbf{B}^{(n)}. \end{aligned} \quad (\text{B1})$$

For simplicity, we assume that the sizes of $\mathbf{A}^{(n)}$ and $\mathbf{B}^{(n)}$ for $1 \leq n \leq N - 1$ are $(\chi_1 \times \mathcal{D} \times \chi'_1)$ and $(\chi_2 \times \mathcal{D} \times \chi'_2)$, respectively, considering the open boundary conditions. The sizes of $\mathbf{A}^{(1)}$ and $\mathbf{B}^{(1)}$ are $(1 \times \mathcal{D} \times \chi'_1)$ and $(1 \times \mathcal{D} \times \chi'_2)$, respectively. The sizes of $\mathbf{A}^{(N)}$ and $\mathbf{B}^{(N)}$ are $(\chi_1 \times \mathcal{D} \times 1)$ and $(\chi_2 \times \mathcal{D} \times 1)$, respectively. Then the size of $\mathbf{Q}^{(n)}$ is $[(\chi_1 + \chi_2) \times \mathcal{D} \times (\chi'_1 + \chi'_2)]$.

If the dimensions of the left virtual bonds of $\mathbf{A}^{(n)}$ and $\mathbf{B}^{(n)}$ are both one, the above equation can be simplified to

$$\begin{aligned} \mathbf{Q}_{:\chi_1}^{(n)} &= \mathbf{A}^{(n)}, \\ \mathbf{Q}_{:\chi_1}^{(n)} &= \mathbf{B}^{(n)}. \end{aligned} \quad (\text{B2})$$

The size of $\mathbf{Q}^{(n)}$ will be $[1 \times \mathcal{D} \times (\chi'_1 + \chi'_2)]$ instead of $[2 \times \mathcal{D} \times (\chi'_1 + \chi'_2)]$. The same simplification can be made in the case that the dimensions of the right virtual bonds of $\mathbf{A}^{(n)}$ and $\mathbf{B}^{(n)}$ are both one.

Let us now consider less general cases by assuming $\mathbf{A}^{(n)} \neq \mathbf{B}^{(n)}$ only for $n = m$; otherwise, $\mathbf{A}^{(n)} = \mathbf{B}^{(n)}$. In other words, the tensors in the two MPSs are the same except for the m th tensor. Then $\{\mathbf{Q}^{(n)}\}$ satisfy

$$\begin{aligned} \mathbf{Q}^{(n)} &= \mathbf{A}^{(n)} = \mathbf{B}^{(n)} \text{ for } n < m - 1 \text{ or } n > m + 1, \\ \mathbf{Q}_{:\chi_1, \dots, \chi'_1}^{(n)} &= \mathbf{A}^{(n)} \\ \mathbf{Q}_{:\chi_1, \dots, \chi'_1}^{(n)} &= \mathbf{B}^{(n)} \quad \text{for } n = m - 1, \\ \mathbf{Q}_{\chi_1, \dots, \chi'_1}^{(n)} &= \mathbf{A}^{(n)} \\ \mathbf{Q}_{\chi_1, \dots, \chi'_1}^{(n)} &= \mathbf{B}^{(n)} \quad \text{for } n = m + 1, \\ \mathbf{Q}_{\chi_1, \dots, \chi'_1}^{(n)} &= \mathbf{A}^{(n)} \\ \mathbf{Q}_{\chi_1, \dots, \chi'_1}^{(n)} &= \mathbf{B}^{(n)} \quad \text{otherwise.} \end{aligned} \quad (\text{B3})$$

The size of $\mathbf{Q}^{(n)}$ for $n < m - 1$ or $n > m + 1$ is $(\chi_1 \times \mathcal{D} \times \chi'_1)$, the same as $\mathbf{A}^{(n)}$ or $\mathbf{B}^{(n)}$, which equal each other in this case. The size of $\mathbf{Q}^{(n)}$ for $n = m - 1$ is $[\chi_1 \times \mathcal{D} \times (\chi'_1 + \chi'_2)]$. The size for $n = m + 1$ is $[(\chi_1 + \chi_2) \times \mathcal{D} \times \chi'_1]$. Otherwise, the size of $\mathbf{Q}^{(n)}$ is $[(\chi_1 + \chi_2) \times \mathcal{D} \times (\chi'_1 + \chi'_2)]$.

APPENDIX C: INNER PRODUCT OF MATRIX PRODUCT STATES

Given two MPSs formed by tensors $\{\mathbf{A}^{(n)}\}$ and $\{\mathbf{B}^{(n)}\}$ ($n = 1, \dots, N$), their inner product is defined as

$$\begin{aligned} z &= \sum_{s_1 \dots s_N} \sum_{\substack{a_0 \dots a_N \\ a'_0 \dots a'_N}} A_{\alpha_0 s_1 \alpha_1}^{(1)} A_{\alpha_1 s_2 \alpha_2}^{(2)} \dots A_{\alpha_{N-1} s_N \alpha_N}^{(N)} \\ &\quad \times B_{\alpha'_0 s_1 \alpha'_1}^{(1)} B_{\alpha'_1 s_2 \alpha'_2}^{(2)} \dots B_{\alpha'_{N-1} s_N \alpha'_N}^{(N)}. \end{aligned} \quad (\text{C1})$$

Equation (C1) can be calculated in an iterative way. We start with a matrix \mathbf{V} whose size is $\dim(\alpha_1) \times \dim(\alpha'_1)$ and take $V_{0,0} = 1$ [note $\dim(\alpha_1) = \dim(\alpha'_1) = 1$]. We update \mathbf{V} by

$$V_{\alpha_n \alpha'_n} \leftarrow \sum_{s_n \alpha_{n-1} \alpha'_{n-1}} V_{\alpha_{n-1} \alpha'_{n-1}} A_{\alpha_{n-1} s_n \alpha_n}^{(n)} B_{\alpha'_{n-1} s_n \alpha'_n}^{(n)}. \quad (\text{C2})$$

We iteratively calculate \mathbf{V} by taking n from 1 to N , and finally, \mathbf{V} becomes a (1×1) matrix (i.e., a scalar) since $\dim(\alpha_N) = \dim(\alpha'_N) = 1$. We have

$$z = V_{0,0}. \quad (\text{C3})$$

An efficient way to calculate Eq. (C2) is to first compute $\tilde{A}_{\alpha'_{n-1} s_n \alpha_n} = \sum_{\alpha_{n-1}} V_{\alpha_{n-1} \alpha'_{n-1}} A_{\alpha_{n-1} s_n \alpha_n}^{(n)}$ and then $V_{\alpha_n \alpha'_n} = \sum_{s_n \alpha'_{n-1}} \tilde{A}_{\alpha'_{n-1} s_n \alpha_n} B_{\alpha'_{n-1} s_n \alpha'_n}^{(n)}$. The complexities of these two scale, respectively, as

$$O[\dim(\alpha'_{n-1}) \dim(\alpha_{n-1}) \dim(s_n) \dim(\alpha_n)], \quad (\text{C4})$$

$$O[\dim(\alpha'_{n-1}) \dim(\alpha'_n) \dim(\alpha_n) \dim(s_n)]. \quad (\text{C5})$$

Thus, the complexity of calculating Eq. (C2) scales as

$$O\{\dim(s_n) \dim(\alpha'_{n-1}) \dim(\alpha_n) [\dim(\alpha_{n-1}) + \dim(\alpha'_n)]\}. \quad (\text{C6})$$

The above method can be used to calculate the norm of a given MPS, which equals \sqrt{z} .

- [1] P. Geerlings, F. De Proft, and W. Langenaeker, Conceptual density functional theory, *Chem. Rev.* **103**, 1793 (2003).
- [2] P. Carsky and M. Urban, *Ab Initio Calculations: Methods and Applications in Chemistry*, Lecture Notes in Chemistry, Vol. 16 (Springer, Des Moines, Iowa USA, 2012)
- [3] K. T. Schütt, M. Gastegger, A. Tkatchenko, K.-R. Müller, and R. J. Maurer, Unifying machine learning and quantum chemistry with a deep neural network for molecular wavefunctions, *Nat. Commun.* **10**, 5024 (2019).
- [4] J. Han, L. Zhang, and Weinan E, Solving many-electron Schrödinger equation using deep neural networks, *J. Comput. Phys.* **399**, 108929 (2019).
- [5] J. Hermann, Z. Schätzle, and F. Noé, Deep-neural-network solution of the electronic Schrödinger equation, *Nat. Chem.* **12**, 891 (2020).
- [6] S. Manzhos, Machine learning for the solution of the Schrödinger equation, *Mach. Learn.: Sci. Technol.* **1**, 013002 (2020).
- [7] K. Choo, A. Mezzacapo, and G. Carleo, Fermionic neural-network states for ab-initio electronic structure, *Nat. Commun.* **11**, 2368 (2020).
- [8] A. Sehanobish, H. H. Corzo, O. Kara, and D. van Dijk, Learning potentials of quantum systems using deep neural networks, in *Proceedings of the AAAI 2021 Spring Symposium on Combining Artificial Intelligence and Machine Learning with Physical Sciences*, Vol. 2964 (AAAI, 2021), p. 0074-2964-3.
- [9] R. Hong, P.-F. Zhou, B. Xi, J. Hu, A.-C. Ji, and S.-J. Ran, Predicting quantum potentials by deep neural network and metropolis sampling, *SciPost Phys. Core* **4**, 022 (2021).
- [10] C. Verdi, F. Karsai, P. Liu, R. Jinnouchi, and G. Kresse, Thermal transport and phase transitions of zirconia by on-the-fly machine-learned interatomic potentials, *npj Comput. Mater.* **7**, 156 (2021).
- [11] M. Wieder, J. Fass, and J. D. Chodera, Fitting quantum machine learning potentials to experimental free energy data: Predicting tautomer ratios in solution, *Chem. Sci.* **12**, 11364 (2021).
- [12] F. Verstraete, V. Murg, and J. I. Cirac, Matrix product states, projected entangled pair states, and variational renormalization group methods for quantum spin systems, *Adv. Phys.* **57**, 143 (2008).
- [13] J. I. Cirac and F. Verstraete, Renormalization and tensor product states in spin chains and lattices, *J. Phys. A* **42**, 504004 (2009).
- [14] R. Orús, A practical introduction to tensor networks: Matrix product states and projected entangled pair states, *Ann. Phys. (New York)* **349**, 117 (2014).
- [15] S.-J. Ran, E. Tirrito, C. Peng, X. Chen, L. Tagliacozzo, G. Su, and M. Lewenstein, *Tensor Network Contractions: Methods and Applications to Quantum Many-Body Systems* (Springer, Cham, 2020).
- [16] R. Orús, Tensor networks for complex quantum systems, *Nat. Rev. Phys.* **1**, 538 (2019).
- [17] S. R. White, Density Matrix Formulation for Quantum Renormalization Groups, *Phys. Rev. Lett.* **69**, 2863 (1992).
- [18] S. R. White, Density-matrix algorithms for quantum renormalization groups, *Phys. Rev. B* **48**, 10345 (1993).
- [19] U. Schollwöck, The density-matrix renormalization group, *Rev. Mod. Phys.* **77**, 259 (2005).
- [20] U. Schollwöck, The density-matrix renormalization group in the age of matrix product states, *Ann. Phys. (New York)* **326**, 96 (2011).
- [21] E. M. Stoudenmire and S. R. White, Studying two-dimensional systems with the density matrix renormalization group, *Annu. Rev. Condens. Matter Phys.* **3**, 111 (2012).
- [22] F. Verstraete, M. M. Wolf, D. Perez-Garcia, and J. I. Cirac, Criticality, the Area Law, and the Computational Power of Projected Entangled Pair States, *Phys. Rev. Lett.* **96**, 220601 (2006).
- [23] J. Jordan, R. Orús, G. Vidal, F. Verstraete, and J. I. Cirac, Classical Simulation of Infinite-Size Quantum Lattice Systems in Two Spatial Dimensions, *Phys. Rev. Lett.* **101**, 250602 (2008).
- [24] J. Eisert, M. Cramer, and M. B. Plenio, Colloquium: Area laws for the entanglement entropy, *Rev. Mod. Phys.* **82**, 277 (2010).
- [25] Y. Ge and J. Eisert, Area laws and efficient descriptions of quantum many-body states, *New J. Phys.* **18**, 083026 (2016).
- [26] F. Verstraete and J. I. Cirac, Matrix product states represent ground states faithfully, *Phys. Rev. B* **73**, 094423 (2006).
- [27] M. Dolfi, B. Bauer, M. Troyer, and Z. Ristivojevic, Multigrid Algorithms for Tensor Network States, *Phys. Rev. Lett.* **109**, 020604 (2012).
- [28] E. M. Stoudenmire and S. R. White, Sliced Basis Density Matrix Renormalization Group for Electronic Structure, *Phys. Rev. Lett.* **119**, 046401 (2017).
- [29] M. Lubasch, P. Moinier, and D. Jaksch, Multigrid renormalization, *J. Comput. Phys.* **372**, 587 (2018).
- [30] S. Dutta, A. Buyskikh, A. J. Daley, and E. J. Mueller, Density-matrix renormalization group for continuous quantum systems, *arXiv:2108.05366*.

- [31] N. Gourianov, M. Lubasch, S. Dolgov, Q. Y. van den Berg, H. Babae, P. Givi, M. Kiffner, and D. Jaksch, A Quantum Inspired Approach to Exploit Turbulence Structures, *Nat. Comput. Sci.* **2**, 30 (2022).
- [32] F. Verstraete and J. I. Cirac, Continuous Matrix Product States for Quantum Fields, *Phys. Rev. Lett.* **104**, 190405 (2010).
- [33] J. Haegeman, J. I. Cirac, T. J. Osborne, and F. Verstraete, Calculus of continuous matrix product states, *Phys. Rev. B* **88**, 085118 (2013).
- [34] A. Steffens, C. A. Riofrio, R. Hübener, and J. Eisert, Quantum field tomography, *New J. Phys.* **16**, 123010 (2014).
- [35] D. Jennings, C. Brockett, J. Haegeman, T. J. Osborne, and F. Verstraete, Continuum tensor network field states, path integral representations and spatial symmetries, *New J. Phys.* **17**, 063039 (2015).
- [36] A. Tilloy and J. I. Cirac, Continuous Tensor Network States for Quantum Fields, *Phys. Rev. X* **9**, 021040 (2019).
- [37] A. E. B. Nielsen, B. Herwerth, J. I. Cirac, and G. Sierra, Field tensor network states, *Phys. Rev. B* **103**, 155130 (2021).
- [38] H.-J. Liao, J.-G. Liu, L. Wang, and T. Xiang, Differentiable Programming Tensor Networks, *Phys. Rev. X* **9**, 031041 (2019).
- [39] B. Ph. van Milligen, V. Tribaldos, and J. A. Jiménez, Neural Network Differential Equation and Plasma Equilibrium Solver, *Phys. Rev. Lett.* **75**, 3594 (1995).
- [40] I. E. Lagaris, A. Likas, and D. I. Fotiadis, Artificial neural networks for solving ordinary and partial differential equations, *IEEE Trans. Neural Networks* **9**, 987 (1998).
- [41] S. Mall and S. Chakraverty, Application of Legendre neural network for solving ordinary differential equations, *Appl. Soft Comput.* **43**, 347 (2016).
- [42] Y. Bar-Sinai, S. Hoyer, J. Hickey, and M. P. Brenner, Learning data-driven discretizations for partial differential equations, *Proc. Natl. Acad. Sci. U.S.A.* **116**, 15344 (2019).
- [43] H. Sun, M. Hou, Y. Yang, T. Zhang, F. Weng, and F. Han, Solving partial differential equation based on Bernstein neural network and extreme learning machine algorithm, *Neural Process. Lett.* **50**, 1153 (2019).
- [44] D. P. Kingma and J. Ba, Adam: A method for stochastic optimization, in *3rd International Conference on Learning Representations, ICLR 2015, San Diego, CA, USA, May 7-9, 2015, Conference Track Proceedings* (2015).
- [45] A. Beygi, S. P. Klevansky, and C. M. Bender, Coupled oscillator systems having partial \mathcal{PT} symmetry, *Phys. Rev. A* **91**, 062101 (2015).
- [46] T. Barthel, C. Pineda, and J. Eisert, Contraction of fermionic operator circuits and the simulation of strongly correlated fermions, *Phys. Rev. A* **80**, 042333 (2009).
- [47] P. Corboz, R. Orús, B. Bauer, and G. Vidal, Simulation of strongly correlated fermions in two spatial dimensions with fermionic projected entangled-pair states, *Phys. Rev. B* **81**, 165104 (2010).
- [48] P. Corboz, J. Jordan, and G. Vidal, Simulation of fermionic lattice models in two dimensions with projected entangled-pair states: Next-nearest neighbor Hamiltonians, *Phys. Rev. B* **82**, 245119 (2010).
- [49] I. Pižorn and F. Verstraete, Fermionic implementation of projected entangled pair states algorithm, *Phys. Rev. B* **81**, 245110 (2010).
- [50] S. R. White and R. L. Martin, Ab initio quantum chemistry using the density matrix renormalization group, *J. Chem. Phys.* **110**, 4127 (1999).
- [51] Z.-C. Gu and X.-G. Wen, Tensor-entanglement-filtering renormalization approach and symmetry protected topological order, *Phys. Rev. B* **80**, 155131 (2009).
- [52] N. Schuch, J. I. Cirac, and D. Pérez-García, PEPS as ground states: Degeneracy and topology, *Ann. Phys. (New York)* **325**, 2153 (2010).
- [53] S. Singh, R. N. C. Pfeifer, and G. Vidal, Tensor network decompositions in the presence of a global symmetry, *Phys. Rev. A* **82**, 050301(R) (2010).
- [54] D. Pérez-García, M. Sanz, C. E. González-Guillén, M. M. Wolf, and J. I. Cirac, Characterizing symmetries in a projected entangled pair state, *New J. Phys.* **12**, 025010 (2010).
- [55] I. L. Markov and Y. Shi, Simulating quantum computation by contracting tensor networks, *SIAM J. Comput.* **38**, 963 (2008).
- [56] I. Arad and Z. Landau, Quantum computation and the evaluation of tensor networks, *SIAM J. Comput.* **39**, 3089 (2010).
- [57] K. Fujii and T. Morimae, Computational power and correlation in a quantum computational tensor network, *Phys. Rev. A* **85**, 032338 (2012).
- [58] I. Dhand, M. Engelkemeier, L. Sansoni, S. Barkhofen, C. Silberhorn, and M. B. Plenio, Proposal for Quantum Simulation via All-Optically-Generated Tensor Network States, *Phys. Rev. Lett.* **120**, 130501 (2018).
- [59] C. Huang, F. Zhang, M. Newman, X. Ni, D. Ding, J. Cai, X. Gao, T. Wang, F. Wu, G. Zhang, H.-S. Ku, Z. Tian, J. Wu, H. Xu, H. Yu, B. Yuan, M. Szegedy, Y. Shi, H.-H. Zhao, C. Deng, and J. Chen, Efficient parallelization of tensor network contraction for simulating quantum computation, *Nat. Comput. Sci.* **1**, 578 (2021).